Supporting Information for "Westward-propagating Moisture Mode over the Tropical Western Hemisphere"

Víctor C. Mayta[1,2] *, Ángel F. Adames [1], Fiaz Ahmed [3]

[1]Department of Atmospheric and Oceanic Sciences, University of Wisconsin, Madison, Wisconsin

[2]Department of Climate and Space Science and Engineering, University of Michigan, Ann Arbor, Michigan

[3]Department of Atmospheric and Oceanic Sciences, University of California, Los Angeles, California

Contents of this file

Text S1: Effective Gross Moist Stability (Γ_{eff})

This criteria has been suggested to be important to the growth of slow-propagating systems that have characteristics of moisture modes (Sobel & Maloney, 2013; Inoue &

*Department of Atmospheric and Oceanic Sciences, University of Wisconsin, 1225 W Dayton St, Madison, WI 53706, USA.

Back, 2017; Inoue et al., 2020). Γ_{eff} is a measure of the GMS that includes the impact of the cloud-radiation feedback (Γ_r) on the moisture modes. Thus, moisture modes occur if Γ_{eff} is close to zero or even negative.

In this study, we calculated Γ_{eff} from a scatterplot of anomalous $\langle \omega \partial_p m \rangle$ and $\langle Q_r \rangle$ against $\nabla \cdot \langle s\mathbf{v} \rangle$ as in Inoue and Back (2017):

$$\Gamma_{eff} = \underbrace{\frac{\langle \omega \partial_p m \rangle}{\nabla \cdot \langle s\mathbf{v} \rangle}}_{\Gamma} - \underbrace{\frac{\langle Q_r \rangle}{\nabla \cdot \langle s\mathbf{v} \rangle}}_{\Gamma_r} \tag{S1}$$

Figure S4c shows scatterplots for the Γ_{eff}. We also included in the supplementary material the GMS calculation by using VARANAL data for the GoAmazon 2014/15 field campaign. Γ shows positive values for both datasets with larger anomalies obtained from VARANAL (Table S1). Despite Γ is showing a relatively high value for the intraseasonal westward-propagating (ISWP), the Γ_r parameter is depicting even a higher value, with $\Gamma_r = 0.181$ for ERA5 and $\Gamma_r = 0.125$ for VARANAL, respectively. Thus, from Eq. (S1) and Fig. S4c is possible to infer that the Γ_{eff} results in negative values associated with the ISWP ($\Gamma_{eff} = -0.082$ and $\Gamma_{eff} = -0.018$ for ERA5 and VARANAL, respectively).

Text S2: Equatorial beta-plane model with prognostic moisture and background flow

a. Model setup

We use a similar model as in Ahmed (2021). In addition to the prognostic moisture equation shown in the main text, this model includes a set of equations for the horizontal momentum and column-integrated dry static energy and moisture, as well as the

constraints of hydrostatic balance and mass continuity:

$$\frac{\partial u'}{\partial t} - \beta y v' + \frac{\partial \phi'}{\partial x} = 0 \tag{S2}$$

$$\frac{\partial v'}{\partial t} + \beta y u' + \frac{\partial \phi'}{\partial y} = 0 \tag{S3}$$

$$\frac{\partial u'}{\partial x} + \frac{\partial v'}{\partial y} = -\frac{\partial \omega'}{\partial p} \tag{S4}$$

$$\frac{\partial \phi'}{\partial p} = -\frac{R_d}{p} T' \tag{S5}$$

$$\frac{\partial \langle T' \rangle}{\partial t} + \left\langle \omega \frac{\partial \bar{S}}{\partial p} \right\rangle = \langle Q'_c \rangle + \langle Q'_r \rangle \tag{S6}$$

In the above equation, u', v' and ω' are the perturbation zonal, meridional and vertical pressure velocities respectively. ϕ' is the perturbation geopotential, and T' is the perturbation temperature. The perturbation radiative and convective heating rates are Q'_r and Q'_c, respectively. The background dry static energy is $\bar{S}$, the planetary vorticity gradient is β and R_d is the dry gas constant. Note that the background zonal wind $\bar{U}$, appears in the prognostic moisture equation (Eq. 7 in the main text) but not in the horizontal momentum equations (S2)-(S3). We allow this to make the subsequent derivation easier, and because we only focus on the qualitative aspects of the MSE budget and the horizontal structures. A more complete theory of the moist equatorial Rossby wave must also include momentum advection by the background wind.

We now follow that same reduction procedures as in Ahmed (2021), which are broadly: i) vertical truncation procedures following Neelin and Zeng (2000), ii) using complex exponentials to represent perturbations, and iii) reducing the system to a single second-order ODE.

b. Parameterizations

1. Convection is parameterized using an adjustment based scheme, derived from the observed precipitation-buoyancy relationship (Ahmed & Neelin, 2018; Ahmed et al., 2020):

$$\langle Q_c' \rangle = \epsilon_q \langle q' \rangle - \epsilon_t \langle T' \rangle, \tag{S7}$$

where ϵ_q and ϵ_t are relaxation timescales for column-integrated moisture and temperature respectively. The value for ϵ_q^{-1} is assumed to be 8 hours, slightly longer than the 6 hours used in Ahmed (2021). This reflects the slightly cooler tropospheric temperatures in the western hemisphere (Neelin et al., 2009), which quantitatively impacts the convection's moisture sensitivity (Ahmed et al., 2020). Tests using a range of moisture relaxation timescales from 6 hours to 24 hours did not qualitatively alter our results.

2. Cloud-radiative heating is parameterized with a linear dependence on the convective heating (Su & Neelin, 2002; Peters & Bretherton, 2005):

$$\langle Q_r' \rangle = r \langle Q_c' \rangle, \tag{S8}$$

where r is the cloud radiative heating parameter.

3. The combined effects of zonal moisture advection and surface evaporation are parameterized using a linear dependence on the background wind (Sobel & Maloney, 2013; Adames & Kim, 2016):

$$E' - \langle u' \frac{\partial \bar{q}}{\partial x} \rangle = \sigma_x u_1, \tag{S9}$$

where σ_x is the combined zonal advection and surface evaporation parameter, and u_1 is the horizontal component of the perturbation zonal wind (after vertical truncation). When $\sigma_x > 0$, low-level easterlies anomalously moisten the column. This effect could

arise due to low-level background easterlies or a positive zonal moisture gradient. Since the low-level zonal moisture gradient over the TWH region is negative (not shown), we use a small negative value for σ_x (see Table S1).

4. The meridional moisture advection is parameterized using a quadratic dependence on the north-south distance from the equator. This parameterization yields:

$$\left\langle v' \frac{\partial \bar{q}}{\partial y} \right\rangle = v_1 \sigma_y y, \tag{S10}$$

where σ_y denotes the strength of the background meridional moisture gradient and v_1 is the horizontal component of the perturbation meridional wind.

The reader is referred to Ahmed (2021) for additional details on the parameterization and model derivation.

c. Eigenvalue problem

We now consider the second-order ODE that is the result of the reduction procedures and parameterizations described above:

$$\frac{d^2\tilde{v}_1}{dy^2} - C_0 y \frac{d\tilde{v}_1}{dy} = -\left(C_1 - C_2 y^2\right)\tilde{v}_1. \tag{S11}$$

In (S11), $\tilde{v}_1$ contains the y dependence in the perturbation meridional wind. The coefficients C_0, C_1 and C_2 are given by:

$$C_0 = \frac{\epsilon_q(1+r)}{(\lambda + ik\bar{U})(\lambda + ik\bar{U} + \epsilon_q\Gamma_{eff})M_s}\left[(\lambda + ik\bar{U})\sigma_y + \beta\sigma_x\right] \tag{S12}$$

$$C_1 = \frac{ik\beta}{(\lambda + ik\bar{U})} - \frac{k^2\lambda}{(\lambda + ik\bar{U})} - \frac{c^2\epsilon_q(1+r)\left[\sigma_y(\lambda + ik\bar{U}) + \sigma_x(ik\lambda + \beta)\right]}{(\lambda + ik\bar{U})c^2(\lambda + ik\bar{U} + \epsilon_q\Gamma_{eff})M_s} - \frac{\lambda(\lambda + ik\bar{U})[(\lambda + ik\bar{U}) + \epsilon_a]}{c^2(\lambda + ik\bar{U} + \epsilon_q\Gamma_{eff})} \tag{S13}$$

$$C_2 = \frac{\beta^2[(\lambda + ik\bar{U}) + \epsilon_a]}{c^2(\lambda + ik\bar{U} + \epsilon_q\Gamma_{eff})} - \frac{ik\beta\epsilon_q(1+r)\sigma_y}{(\lambda + ik\bar{U})(\lambda + ik\bar{U} + \epsilon_q\Gamma_{eff})M_s} \tag{S14}$$

In the above expression, λ and k are the frequency and wavenumber respectively. The other parameters are detailed in Table S1. The coefficients in (S12)–(S14) are similar to those in Ahmed (2021) with the main difference of the frequency λ being replaced by the Doppler shifted frequency $\lambda + ik\bar{U}$. Expressions for the dispersion relationship and the horizontal structures for the state variables—u', v', $\langle T' \rangle$ and $\langle q' \rangle$—are obtained similarly as in Ahmed (2021).

Note the Γ_{eff} appears in the expressions (S12)–(S14) above. In the linear model, we take $\Gamma_{eff} = 0.1$, which is different from the estimate in Text S1. The positive value of Γ_{eff} in the linear model reflects the fact that the time-invariant background state is stable to convection. The slight negative value for Γ_{eff} from Text S1, on the other hand, possibly captures the instability associated with transient convection associated with the ISWP. This distinction is elaborated in Inoue and Back (2017) in their discussion surrounding time-dependent and quasi time independent estimates of the gross moist stability.

d. The MSE budget

Combining the thermodynamic equations: the temperature budget (Eq. S6 from Text S2) and the moisture budget (Eq. 6 in the main text), yields the column-integrated MSE equation,

$$\langle \frac{\partial m'}{\partial t} \rangle = E + \langle Q_r \rangle - \langle \omega' \frac{\partial \bar{m}}{\partial p} \rangle - \langle u' \frac{\partial \bar{q}}{\partial x} \rangle - \langle v' \frac{\partial \bar{q}}{\partial y} \rangle - \langle \bar{U} \frac{\partial q'}{\partial x} \rangle, \tag{S15}$$

where m' is the perturbation column-integrated MSE. Assuming that the perturbations in (S15) can be represented by complex exponentials and using the parameterizations

described in Text S2b yields:

$$\langle \frac{\partial m'}{\partial t} \rangle = \sigma_x u_1 - \sigma_y v_1 y \langle Q_r \rangle + \omega_1 \Gamma M_s - ik\bar{U}\langle q' \rangle, \tag{S16}$$

where ω_1 contains the horizontal dependence in perturbation vertical velocity.

References

Adames, Á. F., & Kim, D. (2016). The MJO as a Dispersive, Convectively Coupled Moisture Wave: Theory and Observations. *Journal of the Atmospheric Sciences*, *73*(3), 913 - 941. doi: 10.1175/JAS-D-15-0170.1

Ahmed, F. (2021). The MJO on the Equatorial Beta Plane: An Eastward-Propagating Rossby Wave Induced by Meridional Moisture Advection. *Journal of the Atmospheric Sciences*, *78*(10), 3115 - 3135. doi: 10.1175/JAS-D-21-0071.1

Ahmed, F., Adames, Á. F., & Neelin, J. D. (2020). Deep Convective Adjustment of Temperature and Moisture. *Journal of the Atmospheric Sciences*, *77*(6), 2163-2186. doi: 10.1175/JAS-D-19-0227.1

Ahmed, F., & Neelin, J. D. (2018). Reverse Engineering the Tropical Precipitation–Buoyancy Relationship. *J. Atmos. Sci.*, *75*(5), 1587-1608. doi: 10.1175/JAS-D-17-0333.1

Dias, J., & Kiladis, G. N. (2014). Influence of the basic state zonal flow on convectively coupled equatorial waves. *Geophysical Research Letters*, *41*(19), 6904–6913. Retrieved from `http://dx.doi.org/10.1002/2014GL061476` doi: 10.1002/2014GL061476

Inoue, K., Adames, Á. F., & Yasunaga, K. (2020). Vertical Velocity Profiles in Convectively Coupled Equatorial Waves and MJO: New Diagnoses of Vertical Velocity

Profiles in the Wavenumber-Frequency Domain. *Journal of the Atmospheric Sciences*, *77*(6), 2139 - 2162. doi: 10.1175/JAS-D-19-0209.1

Inoue, K., & Back, L. E. (2017). Gross Moist Stability Analysis: Assessment of Satellite-Based Products in the GMS Plane. *J. Atmos. Sci.*, *74*(6), 1819-1837. doi: 10.1175/JAS-D-16-0218.1

Mayta, V. C., Kiladis, G. N., Dias, J., Dias, P. L. S., & Gehne, M. (2021). Convectively Coupled Kelvin Waves Over Tropical South America. *Journal of Climate*, *34*(16), 6531 - 6547. doi: 10.1175/JCLI-D-20-0662.1

Neelin, J. D., Peters, O., & Hales, K. (2009). The transition to strong convection. *Journal of the Atmospheric Sciences*, *66*(8), 2367–2384.

Neelin, J. D., & Zeng, N. (2000). A Quasi-Equilibrium Tropical Circulation Model; Formulation. *Journal of the Atmospheric Sciences*, *57*, 1741–1766.

Peters, M. E., & Bretherton, C. S. (2005). A simplified model of the Walker circulation with an interactive ocean mixed layer and cloud-radiative feedbacks. *J. Climate*, *18*(20), 4216–4234.

Sobel, A., & Maloney, E. (2013). Moisture Modes and the Eastward Propagation of the MJO. *Journal of the Atmospheric Sciences*, *70*(1), 187 - 192. doi: 10.1175/JAS-D-12-0189.1

Su, H., & Neelin, J. D. (2002). Teleconnection mechanisms for tropical Pacific descent anomalies during El Niño. *Journal of the atmospheric sciences*, *59*(18), 2694–2712.

Wheeler, M., & Kiladis, G. (1999). Convectively-coupled equatorial waves: Analysis of clouds in the wavenumber-frequency domain. *J. Atmos. Sci.*, *56*, 374–399.

Table S1. Description of parameters used in the equatorial beta-plane model.

Parameter	Description	Value	Units
c	Dry gravity wave speed	50	ms^{-1}
Γ_{eff}	Effective gross moist stability	0.1	-
Γ_r	Cloud-radiative feedback parameter	0.2	-
σ_y	Combined zonal advection and surface evaporation parameter	-1.25×10^{-4}	K kg m^{-3}
σ_x	Meridional moisture advection parameter	9×10^{-9}	K kg m^{-4}
M_s	Gross dry stability	3.12×10^4	K kg m^{-2}
ϵ_q^{-1}	Moisture relaxation timescale	8	hours
ϵ_a^{-1}	Effective convective adjustment timescale ($\epsilon_a = \epsilon_q + [1+r]\epsilon_t$.)	1.4	hours

Table S2. Values of vertical GMS (Γ), cloud-radiation feedback (Γ_r), and the effective GMS (Γ_{eff}) for the ISWP mode.

	Γ	Γ_r	Γ_{eff}
ISWP (ERA5)	0.098	0.181	-0.082
ISWP (Varanal)	0.107	0.125	-0.018

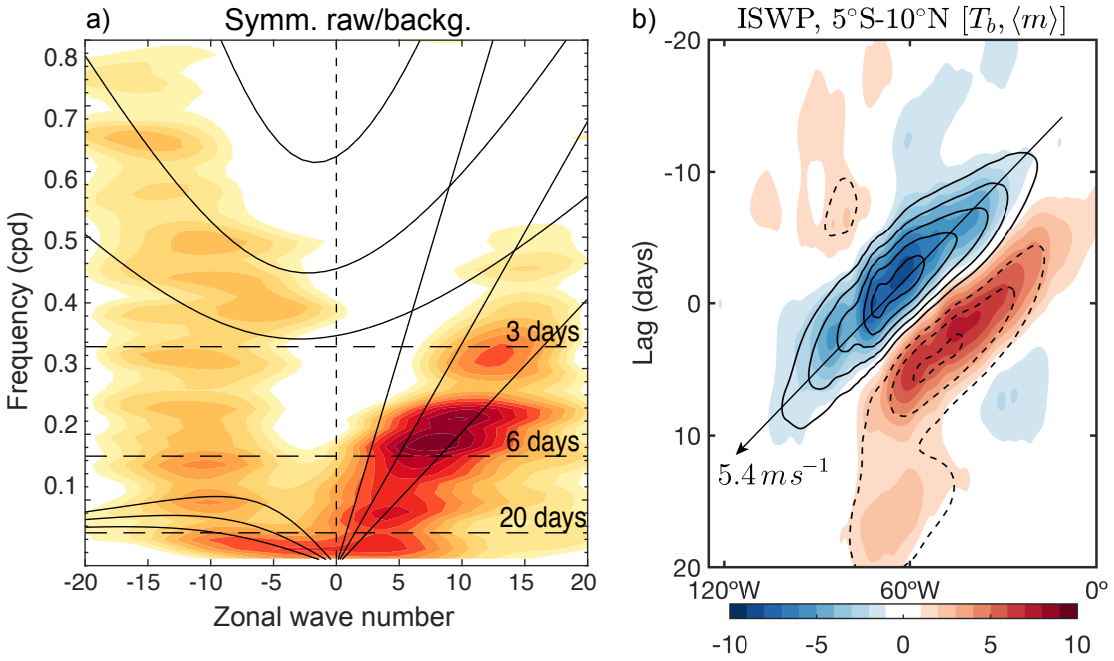

Figure S1. (a) Regional space-time spectra of CLAUS T_b calculated for 10°N–10°S and 120°W–0°. The functional form of the tapering window is the same as described in Wheeler and Kiladis (1999). Background spectra was estimated separately for the regional domain, using the smoothing procedure of Dias and Kiladis (2014). (b) Time-longitude diagram of 5°S–10°N column–integrated MSE (contour) and CLAUS T_b (shading) regressed onto PC1 (normalized, ISWP). The contour interval for $\langle m \rangle$ is $1{\times}10^6$ J m^{-2}.

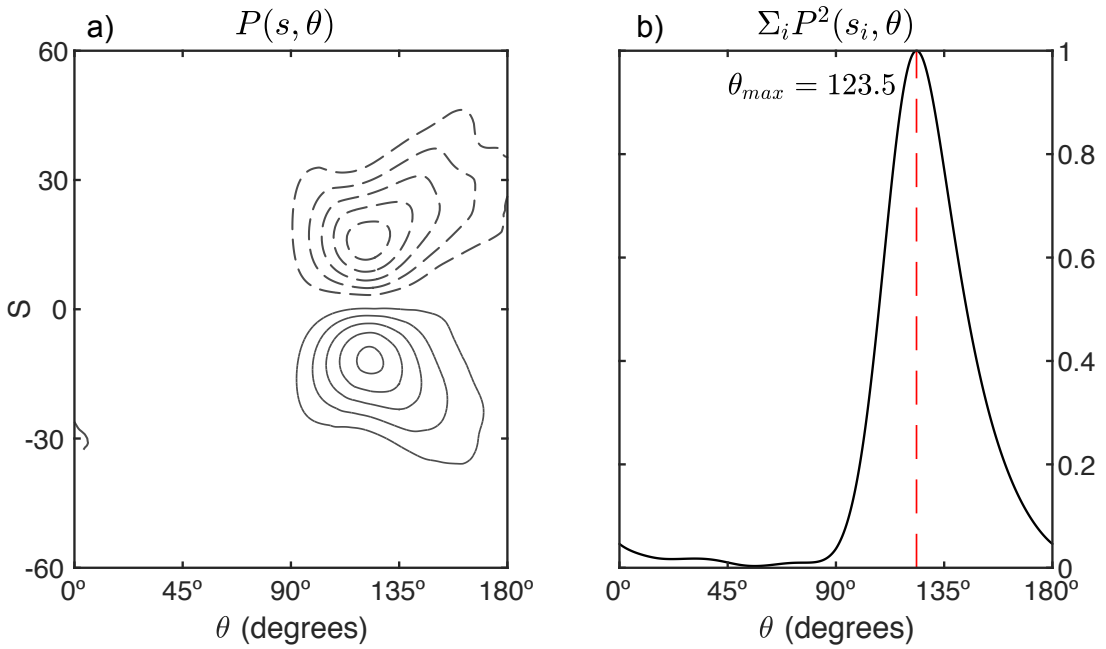

Figure S2. (a) The Radon Transform of the ISWP mode over the Western Hemisphere domain as a function of S and θ. (b) Distribution of the sum-of-squares of the Radon Transform versus θ, normalized such that the maximum value equals 1. The red dashed lines represent the θ_{max} of Eq. A3 in Mayta et al. (2021).

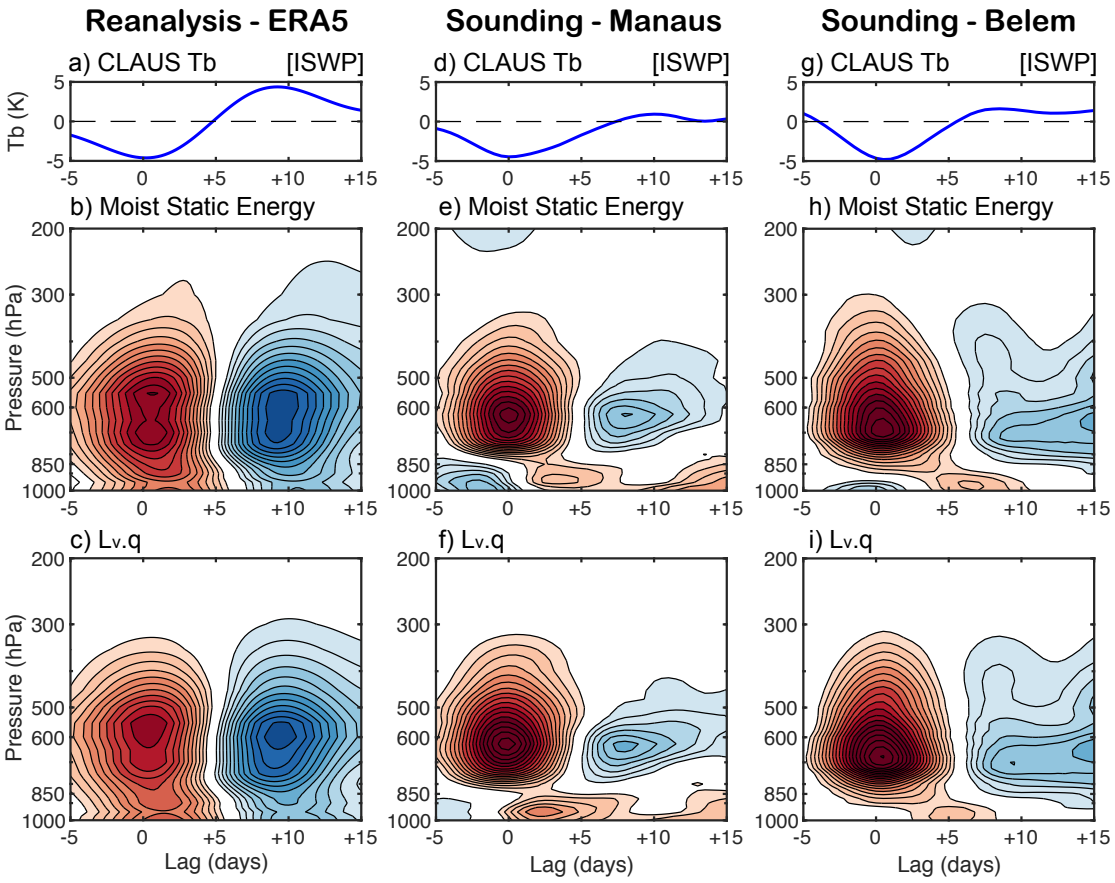

Figure S3. Composite vertical profile of moist static energy (second row) and $L_v \cdot q$ (third row). For reanalysis ERA5 data (panels b and c) is computed as a meridional average (5°S - 10°N) at 60°W. Cross sections in (e),(f) and (h),(i) are computed at Manaus (59.98°W, 3.15°S), and Belem (48.48°W, 1.48°S), respectively. Red and blue shading indicate positive and negative anomalies. The associated T_b anomaly in K is shown at the top. Considering that the Manaus and Belem stations are located at 3.15°S and 1.48°S, respectively, neither station adequately represents the vertical structure that is seen in the reanalysis.

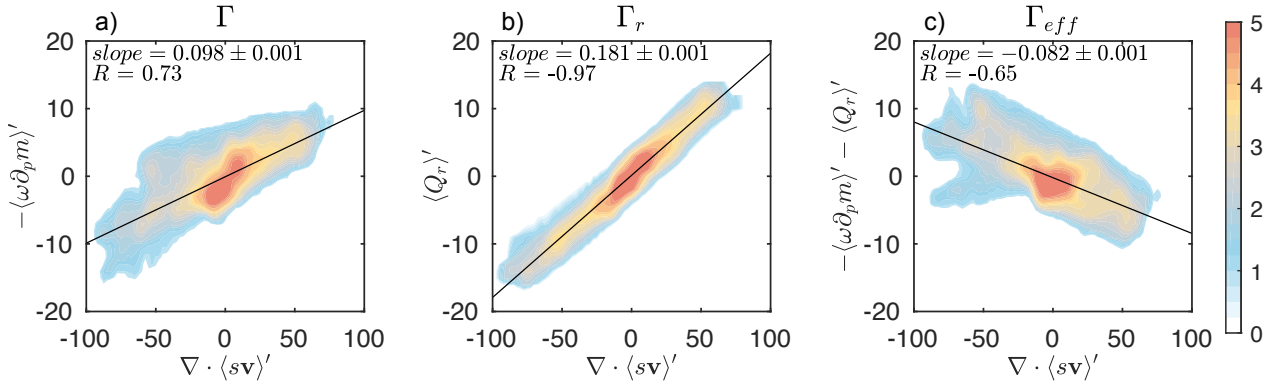

Figure S4. Scatterplots of (a) vertical GMS (Γ), (b) cloud-radiation feedback (Γ_r), and (c) the effective GMS Γ_{eff}. The shading represents the base-10 logarithm of the number of points within 1 W m^{-2} × 5 W m^{-2} bins. Anomalies are computed over western hemisphere (120°–0°,5°S–10°N). The linear fit obtained from linear least squares fit is shown as a solid black line. The slope of the linear fit and the correlation coefficient are shown in the top-left of each panel.

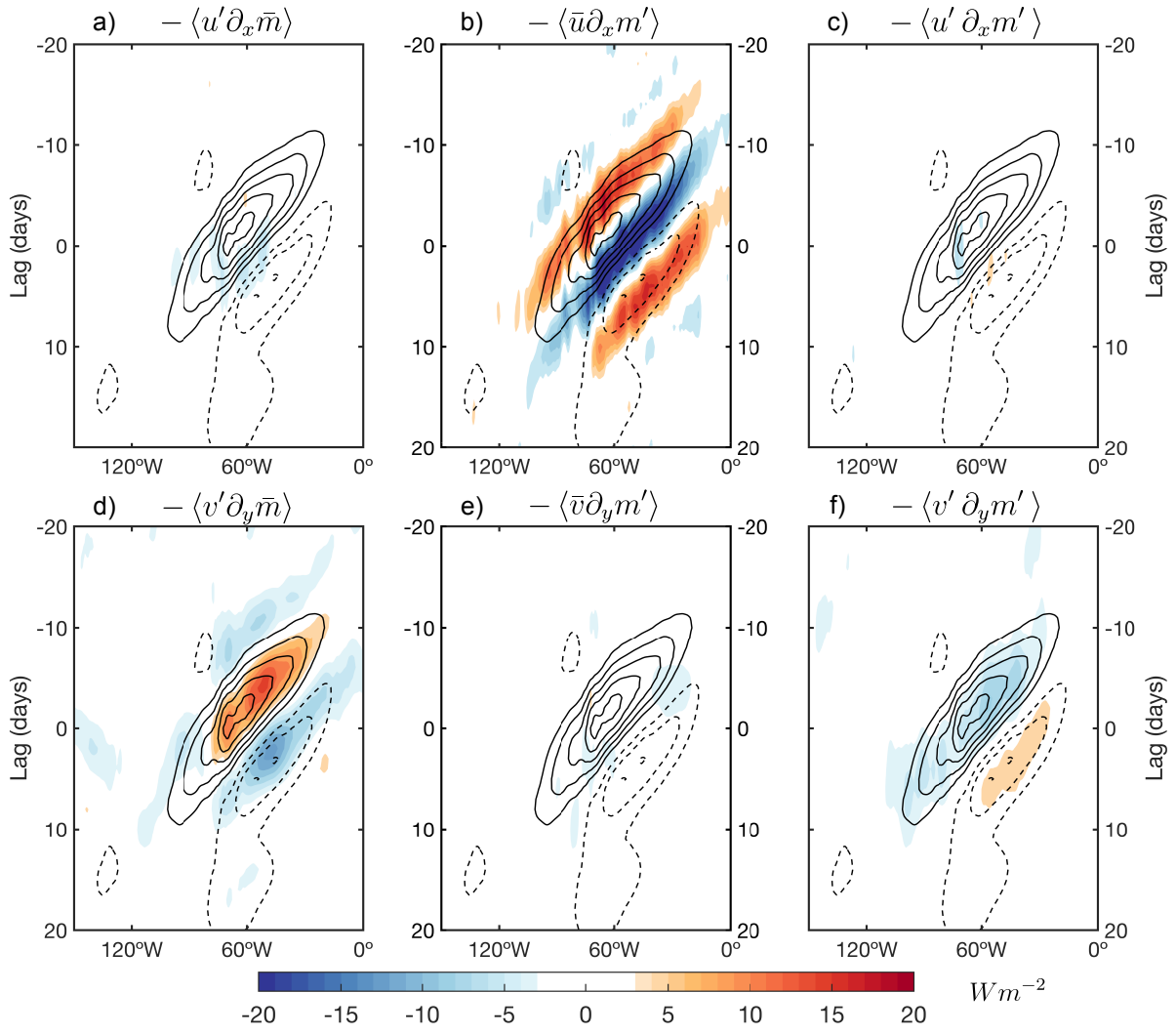

Figure S5. Time-longitude diagram of 5°S - 10°N column–integrated MSE (contour) and horizontal MSE advection components (shading) regressed onto PC1 (normalized, ISWP). (top) Zonal MSE advection terms: (a) $-\langle u'\partial_x\bar{m}\rangle$, (b) $-\langle \bar{u}\partial_x m'\rangle$, (c) $-\langle u'\partial_x m'\rangle$. (bottom) Meridional MSE advection terms: (d) $-\langle v'\partial_y\bar{m}\rangle$, (e) $-\langle \bar{v}\partial_y m'\rangle$, (f) $-\langle v'\partial_y m'\rangle$. The contour interval for $\langle m\rangle$ is 2×10^5 J$\cdot$ m^{-2}.

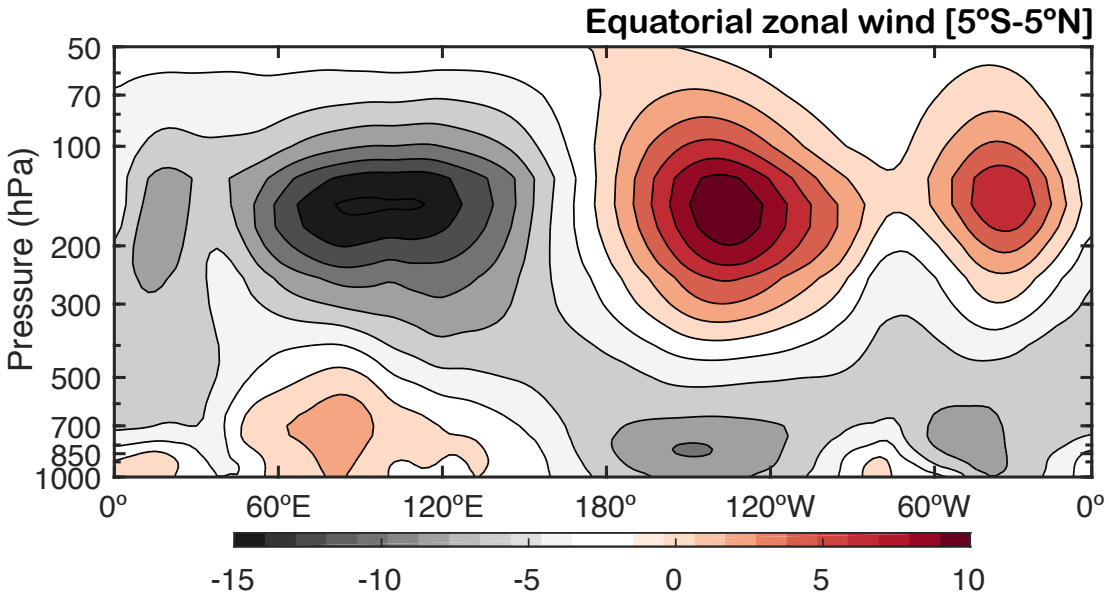

Figure S6. Time-height section of ERA5 equatorial (5°S–5°N) average zonal wind (u) for all-year-season and the 1984–2015 period.